Nonlinear Dyn (2023) 111:22551–22565
https://doi.org/10.1007/s11071-023-08994-7

ORIGINAL PAPER

When do chemical synapses modulate the formation of spiral waves?

Dorsa Nezhad Hajian · Fatemeh Parastesh · Karthikeyan Rajagopal · Sajad Jafari · Matjaž Perc

Received: 14 September 2023 / Accepted: 5 October 2023 / Published online: 30 October 2023

Abstract We study the formation and suppression of spiral wave patterns in a lattice of memristive FitzHugh–Nagumo neurons that are connected through chemical coupling. While earlier works focused predominantly on diffusive coupling, we focus on various parameters that determine the properties of chemical synapses, in particular their firing threshold, the sigmoidal slope, and the reversal potential. Based on physiologically plausible scenarios, we also aim to determine the most probable realistic values of these parameters that facilitate the formation of spiral waves. Furthermore, we study the destabilizing impact of external direct and Faradaic currents on spiral wave patterns, showing that they commonly convert into other turbulent patterns or vanish altogether. Interestingly, however, during the destabilization process, counter-rotating spirals that then collide and generate complex patterns can also be observed.

Keywords Spiral wave · Chemical coupling · Memristive FitzHugh–Nagumo

D. N. Hajian · S. Jafari
Department of Biomedical Engineering, Amirkabir University of Technology (Tehran Polytechnic), Tehran, Iran

F. Parastesh · K. Rajagopal
Centre for Nonlinear Systems, Chennai Institute of Technology, Chennai 600069, Tamil Nadu, India

S. Jafari
Health Technology Research Institute, Amirkabir University of Technology (Tehran Polytechnic), Tehran, Iran

M. Perc
Faculty of Natural Sciences and Mathematics, University of Maribor, Koroška cesta 160, 2000 Maribor, Slovenia

M. Perc
Department of Medical Research, China Medical University Hospital, China Medical University, Taichung 404332, Taiwan

M. Perc
Alma Mater Europaea, Slovenska ulica 17, 2000 Maribor, Slovenia

M. Perc
Complexity Science Hub Vienna, Josefstädterstraße 39, 1080 Vienna, Austria

M. Perc (✉)
Department of Physics, Kyung Hee University, 26 Kyungheedae-ro, Dongdaemun-gu, Seoul, Republic of Korea
e-mail: matjaz.perc@gmail.com

1 Introduction

The nervous system is capable of a wide array of functions, from selective signal amplification [1,2] and encoding messages in firing patterns [3] to efficient signal transmission in the form of spatiotemporal patterns. The emergence of traveling wave patterns in networks of interconnected neurons has captivated researchers' attention for decades. The complex interactions of neural ensembles within the brain generate rich patterns of oscillations in time and space [4,5]. The self-organizing characteristics of the collective electri-

cal activity of neuronal populations offer insights into cognition [6], perception [7], somatosensory [8] mechanism, and task-dependent cortical activities [9]. In planar neuronal arrays, the interplay between excitatory and inhibitory interactions [10], or even disinhibition [11], can form spiral-shaped traveling waves that rotate around a self-sustaining center known as the rotor. The extremities of a traveling wave front are believed to create spiral rotors [12]. Evidence suggests persistent seizures may manifest as recurrent spiral waves propagating in the neocortex [13]. Thus, the formation of spiral waves is often associated with dysfunction. A rich literature also exists on the association between spiral waves and cardiac arrhythmia, with findings suggesting involvement at both cellular and sub-cellular levels [14]. Specifically during ventricular fibrillation, the electrical activity of the heart is predominantly governed by multiple stable spiral rotors [15]. Consequently, efforts have been made to identify tissue properties that foster stable rotors, with the ultimate goal of disrupting these patterns to restore healthy tissue function.

A certain excitability level is required for coupled neuronal ensembles to support wave propagation [16,17]. In forming spiral waves, the fine-tuned excitability of neurons can be provided by an appropriate initial condition set [18,19], external stimulation [20], or tuning system parameters [21] might only be limited to a group of neural oscillators or can be considered in the whole lattice. Single-core stable spiral waves are believed to be born from the high excitability of neurons surrounding the rotor's location, damping the less excited seeds [22]. The generation of spiral waves by blocking traveling waves through the placement of defects can also be inferred as the collision of excited wavefronts and less excited, inhibited, or even silenced sites [23]. Numerous techniques have also been employed to suppress spiral waves. Magnetic induction [24], changing the medium excitability through ionic channels conductivity [25,26], and introducing a certain level of random perturbations [27,28] are a multitude of techniques employed to destabilize and terminate spiral waves. Depending on how it affects network excitability, some factors exhibit a dual behavior as they can either suppress or induce spiral waves [20,29].

Synaptic input properties have shown great potential in the birth and death of spiral waves [30,31]. In electrical synapses, neurons are coupled linearly via their membrane potentials [32], known as diffusive coupling in the literature [33]. It represents the direct exchange of charged ions from one neuron to another through pores known as gap junctions [34]. In contrast, within the chemical synapse, electrical activity is unidirectionally transferred from the presynaptic terminal to the postsynaptic terminal by chemical mediators. A nonlinear sigmoidal function realizes such a connection. Although the chemical synapse does not provide the intercellular continuity or direct exchange of charge as in gap junctions [35], the common saturation effects seen in neurotransmitter–receptor interactions are effectively mirrored through the S-shaped curve of the sigmoidal function [36].

Most research on traveling spiral waves focuses on electrically coupled neuron lattices rather than chemical ones. Reference [37] provides evidence of the emergence of spiral patterns in a planar network of Morris–Lecar neurons, coupled via fast inhibitory and excitatory chemical synapses. It highlights the influential role of excitatory AMPA synapses in spirals' formation. A few works have considered synaptic current constructed of chemical variables and Heaviside function saturation for reporting the spiral waves [30,38]; however, a diffusive voltage term was also involved.

In this exploration, we delve into detecting spiral waves in a lattice of chemically coupled memristive FitzHugh–Nagumo neurons. We considered a chemical coupling that benefits from sigmoidal nonlinearity, and the direct diffusive interactions are intentionally neglected to examine the effect of synapse discontinuity on spiral core formation, stability, and sustained propagation. By unraveling the contributive aspects of sigmoidal activation, firing threshold, and reversal potential of a chemical synapse, we aim to deepen our comprehension of the nature of interactions in neural networks on the birth spiral waves. The destabilizing effects of external and memristive-induced Faradic currents are also reported.

The rest of this paper is organized as follows. Section 2 describes the nodal dynamic, parameter implementation, and synaptic connection. The initial condition, providing a proper level of excitability, is also presented. Section 3 presents the results of spiral wave generation by assessing the parametric configuration of chemical synapses. The destabilizing and suppressing effects of external direct and memristive-induced Faradic currents are reported by employing the condi-

tions under which a single-core spiral is born. Finally, the last section concludes the paper.

2 Methods and models

In the present work, the temporal evolution of planar arrays is ruled by the three-variable memristive Fitzhugh–Nagumo model [39], whose kinetic form is as follows:

$$\begin{aligned}\dot{u}_{ij} &= -ku_{ij}(u_{ij}-a)(u_{ij}-1) - u_{ij}v_{ij} \\ &\quad + k_0\rho(\varphi_{ij})u_{ij} + I_{\text{ext}} + I_{ij}^{\text{syn}}, \\ \dot{v}_{ij} &= \left(\varepsilon + \frac{v_{ij}\mu_1}{u_{ij}+\mu_2}\right)[-v_{ij} - ku_{ij}(u_{ij}-a-1)], \\ \dot{\varphi}_{ij} &= k_1u_{ij} - k_2\varphi_{ij}\end{aligned} \tag{1}$$

where, for the node index (i, j) in the lattice, u_{ij} is transmembrane potential, v_{ij} adjusts the slow current variability, and the third variable φ_{ij} describes the magnetic flux. The excitability of media is tuned by k, ε, μ_1, and μ_2 parameters. In the literature, setting of given parameters are often $k = 8$, $\varepsilon = 0.002$, $a = 0.15$, $\mu_1 = 0.2$, and $\mu_2 = 0.3$ [39]. I_{ext} is the additive external current capable of modulating neurons' excitability and stability of traveling waves. $\rho(\varphi)$ is the nonlinear memductance function of memristor, described by:

$$\rho(\varphi_{ij}) = \frac{\mathrm{d}q(\varphi_{ij})}{\mathrm{d}\varphi_{ij}} = \alpha + 3\beta\varphi_{ij}^{\,2}. \tag{2}$$

For the memristive nonlinear circuit to generate chaotic behavior, the appropriate values of memductance parameters are $\alpha = 0.2$ and $\beta = 0.3$. The parameters k_1 and k_2 are electromagnetic induction gains that are numerically implemented as $k_1 = 0.2$, and $k_2 = 1$ [39]. The additive Faradic current, generated by $\rho(\varphi)u$, modulates the membrane potential by k_0. In the formation of stable traveling spiral waves, the default value of Faradic current gain is tuned to $k_0 = 0.1$, unless stated otherwise. Chemical synapses realize the internodal connections of the lattice. Assuming each node is connected to its eight nearest neighbors, the organized flux of synaptic current injected to the membrane of the neuron (i, j), is described as:

$$\begin{aligned}I_{ij}^{\text{syn}} &= -g_c\left(u_{ij} - V_{\text{rev}}\right) \\ &\quad \times \Big[\Gamma\left(\lambda,\theta,u_{(i+1)j}\right) \\ &\quad + \Gamma\left(\lambda,\theta,u_{(i-1)j}\right) \\ &\quad + \Gamma\left(\lambda,\theta,u_{i(j+1)}\right) + \Gamma\left(\lambda,\theta,u_{i(j-1)}\right) \\ &\quad + \frac{1}{2}\times\Big[\Gamma\left(\lambda,\theta,u_{(i+1)(j+1)}\right) \\ &\quad + \Gamma\left(\lambda,\theta,u_{(i+1)(j-1)}\right) + \Gamma\left(\lambda,\theta,u_{(i-1)(j+1)}\right) \\ &\quad + \Gamma\left(\lambda,\theta,u_{(i-1)(j-1)}\right)\Big]\Big]\end{aligned} \tag{3}$$

where g_c is synaptic connection strength and V_{rev} is reversal potential. The sign of $-g_c\left(u_{ij} - V_{\text{rev}}\right)$ determines the type of coupling, where if positive, the synapse is excitatory, and if negative, it is inhibitory. Note that diagonal connections are half times weaker than axial ones. However, such implementation is unnecessary, considering it shapes a geometrically fine circular wavefront. $\Gamma(\lambda, \theta, u)$ is the sigmoidal nonlinear input–output function of chemical synapse and is as:

$$\Gamma(\lambda,\theta,u) = \frac{1}{1+e^{-\lambda(u-\theta)}}, \tag{4}$$

where λ is the sigmoid slope and θ determines the firing threshold. The function above is also regarded as fast threshold modulation coupling since around the threshold θ, the transition from zero to one smoothly occurs according to slope λ. The greater the sigmoid slope, the sharper the threshold-like behavior gets, resembling a step Heaviside function. In our simulations, the membrane potential is primarily in [0,1] range. Thus, the firing threshold should be rationally selected in the given range.

This paper considers the media in a two-dimensional array of 200×200 nodes. The Euler forward algorithm simulates the three-variable FHN model under no-flux boundary conditions. As the boundary is spatially open, waves tend to leave the plane as they propagate outwards unless the source of propagation remains active in the lattice. However, the reentrant characteristics of spiral rotors succeed in generating sustained traveling in an open lattice.

In the forthcoming sections, the localized initial conditions by which spiral waves appear are selected as $u_0(85:95, 1:100) = 2$, $u_0(96:105, 1:100) = 0.7$,

$u_0(106:110, 1:100) = 0$, $v_0(85:95, 1:100) = 0$,

$v_0(96:105, 1:100) = 0.2$, $v_0(106:110, 1:100) = 0.8$,

$\varphi_0(85:95, 1:100) = 0$, $\varphi_0(96:105, 1:100) = 0.1$, and $\varphi_0(106:115, 1:100) = 0.2$. The rest of the plane initials are set to $u_0 = v_0 = \varphi_0 = 0$. By such arrangement, first, a plane wave travels vertically. Then, the free end of the traveling plane wave swirls around a spatial locus, the interface of the excited and silenced zone at $j = 100$ line. It possibly turns into the spirals' seed after a few iterations. However, the ability of arranged initial states to form stable rotors is closely involved with the synaptic control variables and the degree of excitation provided by external or Faradic current factors. In this context, we take $I_{\text{ext}} = 0$, and $k_0 = 0.1$ to minimize any destabilizing effects.

3 Results

3.1 Birth of spiral waves: the effect of sigmoidal slope λ and firing threshold θ

The beginning of the result section examines the potential effect of sigmoidal steepness around its defined threshold. In the mathematical description of chemical synapses, the response saturation speed is modeled by sigmoid S-curve slope λ, around the operation point of threshold θ. We assume that both λ and θ provide the connection dynamics necessary for the birth of spiral waves.

The response saturation speed of chemical synapses is variable due to the characteristics of the biochemical environment. The neurotransmitter–receptor response saturates at a certain speed regarding the depolarized presynaptic neuron's growing voltage and the postsynaptic terminal's activation threshold. The threshold behavior is believed to be caused by presynaptic efficacy saturation due to the increasing extracellular calcium [40]. The speed of evoked neurotransmitter release and synaptic vesicle fusion process are two factors that determine the synaptic response speed. Evidence suggests that mutations in a specific membrane assembly (SNARE complex protein) accelerate the speed of neurotransmitter release triggered by action potential [41]. Hence, in this work, we seek to numerically assess the undying mechanism of altered saturation speed by λ parameter.

As stated previously, the operating point of biochemical saturation is the response threshold of a chemical synapse. Various physiological scenarios may modulate synaptic threshold. In the context of the electromagnetic field, in vitro studies indicate a modulation of neuronal excitability, with specific observations of hyperpolarized action potential thresholds [42]. Inspired by this study, we aim to explore the potential for the birth of spiral waves in neuronal tissue whose excitability may be influenced by electromagnetic induction. The memristive characteristics of the employed model are contributive to this aim. We begin with a situation in which the firing threshold is relatively high. Then, scenarios of highly excitable neurons are assessed by decreasing the threshold.

Inspired by the abovementioned possibilities, we have studied the formation of stable reentrant waves at different slopes and thresholds of the sigmoid S-curve. For a memristive FHN neuron with $I_{\text{ext}} = 0$, and $k_0 = 0.1$ parameter setting, the membrane potential does not exceed $u = 1$. We begin with situations in which the spiking threshold is relatively high, $\theta = 0.4$, concerning spike peak $u = 1$. Then, we consider $\theta = 0.25$, as a paradigmatical value according to the literature [43,44]. Low thresholds of $\theta = 0.15$ and $\theta = 0.1$ are employed to mimic the hyperpolarized action potential thresholds. For each case, the critical value of λ by which spirals emerge in lattice is assessed. To visualize the geometry of traveling waves, snapshots of the network concerning λ values lower and greater than its critical value are provided. Note that in Figs. 1, 2, 3, and 4, the rest of the synaptic parameters set is as $g_c = 0.02$ and $V_{\text{rev}} = 2.5$. The given value of reversing potential, $V_{\text{rev}} > u_{ij}(t)$ ensures that the type of synaptic coupling is excitatory.

In Fig. 1a, where $\theta = 0.4$, the sigmoid output concerning $u-\lambda$ plane is depicted. As slope λ advances, the sigmoid function gradually transforms into the Heaviside step function, with the zero-to-one (blue to red) transitions occurring suddenly and abruptly. The operating point of transition, which is threshold voltage $\theta = 0.4$, is sketched by black dots. The horizontal white dots specify the minimum sigmoid slope, $\lambda = 9$, by which spiral rotors appear. Concerning the critical value $\lambda = 9$, the snapshots of membrane potential u at $t = 50$, $t = 100$, $t = 250$, and $t = 400$ are provided in Fig. 1b–d, showing the results of $\lambda = 8$, $\lambda = 10$, and $\lambda = 12$, respectively. In Fig. 1b, where $\lambda = 8$, the localized excited region gradually propagates outwards

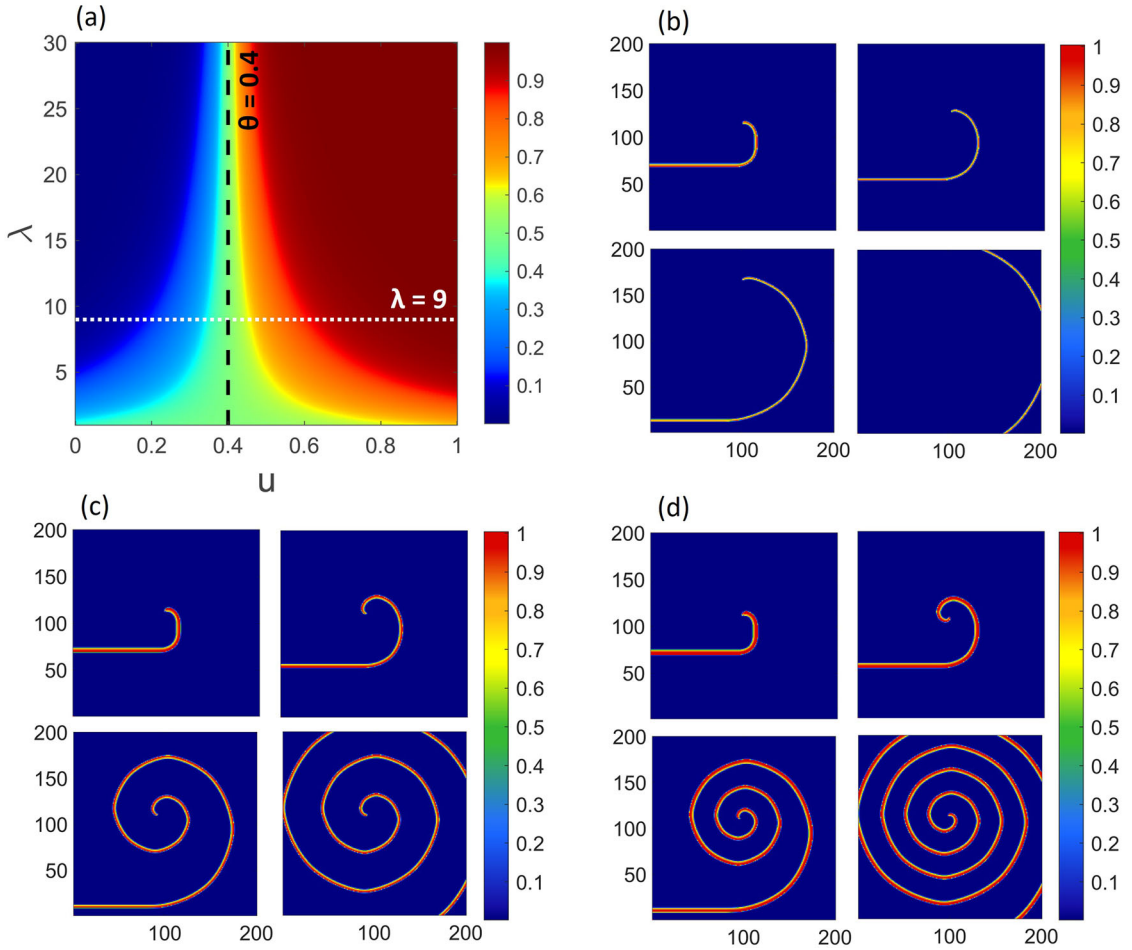

Fig. 1 The effect of the sigmoidal function slope on the formation of stable spiral wavefronts with the firing threshold $\theta = 0.4$. The rest of the synaptic parameters are fixed as $g_c = 0.02$ and $V_{\text{rev}} = 2.5$ ensuring $V_{\text{rev}} > u_{ij}(t)$ for the synapses to be excitatory. Default values of $k_0 = 0.1$ and $I_{\text{ext}} = 0$ are taken. **a** The output of the sigmoidal function concerning the slope of transition $\lambda \in [0, 30]$ and neuron's membrane potential $u \in [0, 1]$. Hot colors specify the synaptic active region. The higher λ is, the transition from synaptic quiescence to firing becomes more abrupt. The minimum λ necessary for a stable rotor emergence is sketched by white dots suggesting $\lambda = 9$. **b** $\lambda = 8$ fails to generate a rotating wavefront due to the weakness of the reentrant tip and the limited space of the lattice. **c** For $\lambda = 10$, the spiral locus is strong enough to sustain. **d** By $\lambda = 12$ stronger wavefronts are formed (the red color indicates the upper range of voltage $u = 1$). (Color figure online)

to excite the rest of the lattice. As expected, the wave rotates inwards for the tip of the traveling wave to interact with the silenced neighboring nodes, initializing the bent wave tip. However, after a few iterations, the bent tip of the traveling wave fails to stabilize and propagates axially rather than reentering itself. In Fig. 1c, where $\lambda = 10$, the bent wavefront turns into a rotating locus, which is spatially stable and keeps reentering itself. The generated rotor is stable enough to shape a single-core stable spiral wave over time. Upon further increasing λ to $\lambda = 12$, once again, stable spirals emerge, yet the wavefronts are stronger than Fig. 1c. By strong wavefront, we mean higher voltage and closer to max $u = 1$, as depicted in red. Figure 1 results suggest that sigmoid smoothness might prevent the formation of spiral rotors while increasing the slope succeeds in supporting stable reentering seeds.

Figure 2 illustrates the impact of the sigmoidal function slope on the formation of stable spiral wavefronts, considering a firing threshold of $\theta = 0.25$.

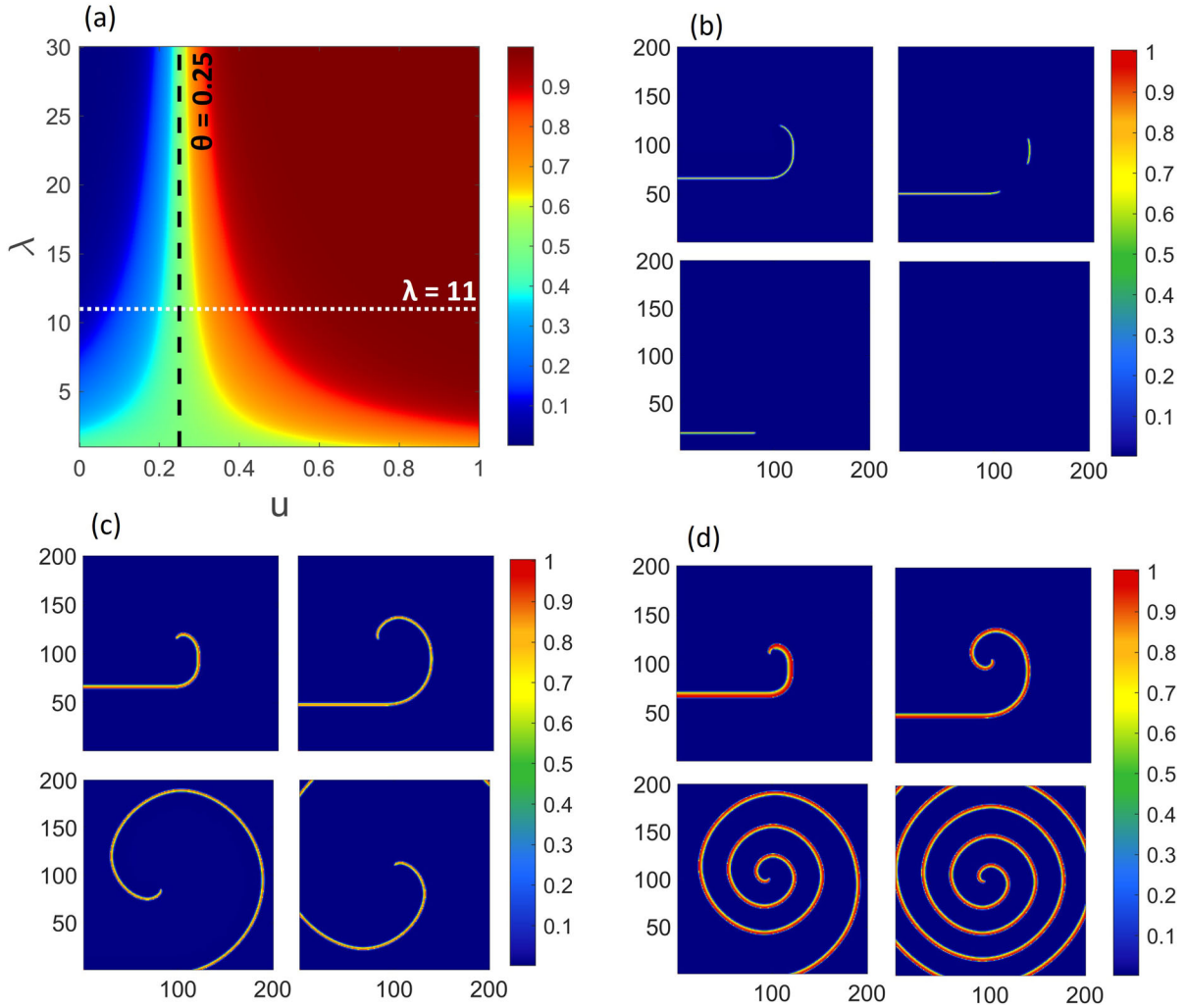

Fig. 2 The effect of the sigmoidal function slope on the formation of stable spiral wavefronts with the firing threshold $\theta = 0.25$. The rest of the synaptic parameter setting is as $g_c = 0.02$ and $V_{\text{rev}} = 2.5$. Default values of $k_0 = 0.1$ and $I_{\text{ext}} = 0$ are taken. **a** The output of the sigmoidal function concerning the slope λ and membrane potential u, the active firing region, gradually begins at threshold $\theta = 0.25$. The minimum λ necessary for the birth of a stable rotor is sketched by white dots suggesting $\lambda = 11$. **b** $\lambda = 10$ fails to generate a rotating wavefront, as the reentrant free end of the traveling wave breaks and the residual plane wave leaves the plane in early iterations. **c** For $\lambda = 12$, the spiral locus is strong enough to sustain. However, the propagating wave of potential is not at its strongest (the traveling wave excites the planar arrays to reach a maximum voltage of $u = 0.7$). **d** By $\lambda = 14$, stronger wavefronts are formed (the red color indicates the upper range of voltage $u = 1$). (Color figure online)

In Fig. 2a, the sigmoidal function's output in $u - \lambda$ plane is demonstrated. The active firing region initiates from the threshold $\theta = 0.25$. In this case, the critical λ for the emergence of a stable rotor is $\lambda = 11$. The snapshots of membrane potential u are taken at $t = 50$, $t = 100$, $t = 250$, and $t = 400$. As depicted in Fig. 2b, $\lambda = 10$ fails to generate a rotating wavefront, leading to the disruption of the reentrant free end of the traveling wave. The residual plane wave drives out of the observable region within the initial iterations. As λ exceeds the critical value, the spiral curved tip survives. A traveling spiral pattern occupies the plane by further inward rotation, as shown in Fig. 2c. At $\lambda = 14$, wavefronts gain strength as the maximum voltage reaches

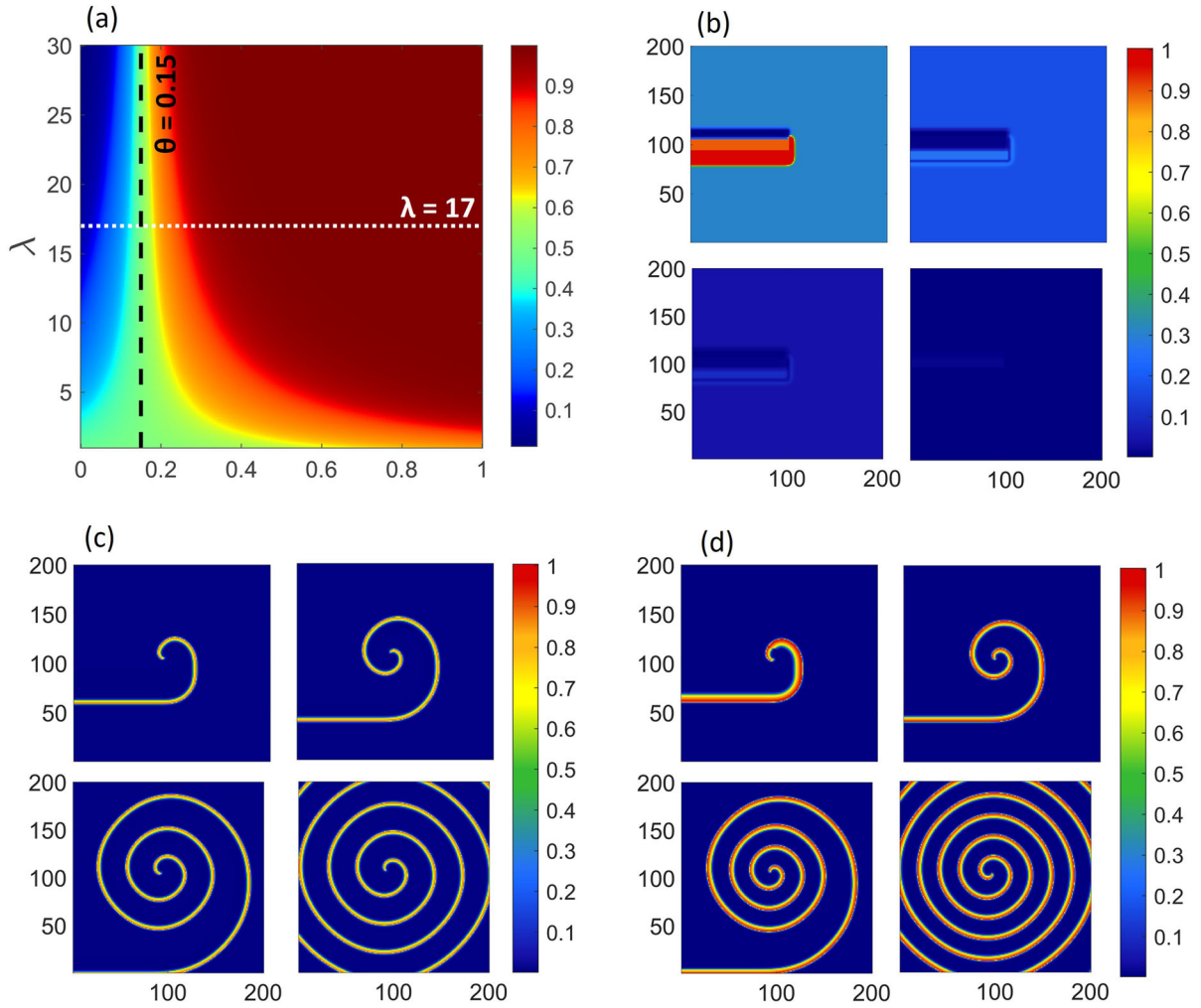

Fig. 3 The effect of the sigmoidal function slope on the formation of stable spiral wavefronts with the firing threshold $\theta = 0.15$. The rest of the synaptic parameter setting is as $g_c = 0.02$ and $V_{\text{rev}} = 2.5$. Default values of $k_0 = 0.1$ and $I_{\text{ext}} = 0$ are taken. **a** The output of the sigmoidal function concerning the slope λ and membrane potential u, the active firing region, gradually begins at $\theta = 0.15$. The minimum required λ for a spiral rotor to appear is sketched by white dots at $\lambda = 17$. **b** By taking $\lambda = 16$, the oscillations become silent shortly after $t = 0$. **c** For $\lambda = 18$, the spiral rotor is born, and wavefronts are strong enough to sustain. **d** By $\lambda = 20$, even stronger wavefronts are formed. (Color figure online)

$u = 1$, and circular wavefronts propagate at lower proximity.

The results of a relatively low-threshold synapse are provided in Fig. 3 as $\theta = 0.15$. Figure 3a presents the output of the sigmoid function, where minimum spiral-forming λ is $\lambda = 17$. The snapshots in Fig. 3b belong to $0 < t < 40$, where $\lambda = 16$. As evident, the free end of the plane wave, originating from the locally excited initial conditions, remains unbent upon interaction with the rest of the lattice. It also fails to propagate vertically and silents soon after $t = 0$. By $t = 40$, the entire lattice reaches a state of equilibrium. For cases 3c, d, snapshots are taken at $t = 40$, $t = 75$, $t = 150$, and $t = 250$. Figure 3c suggests that when λ exceeds the critical value, by being set to $\lambda = 18$, local initials spread to adjacent nodes and form a spiral locus, which is spatially stable. The forthcoming circular wavefronts are also at decent distances, considering the lattice dimensions. In Fig. 3d, by taking $\lambda = 20$, wavefronts are fueled by

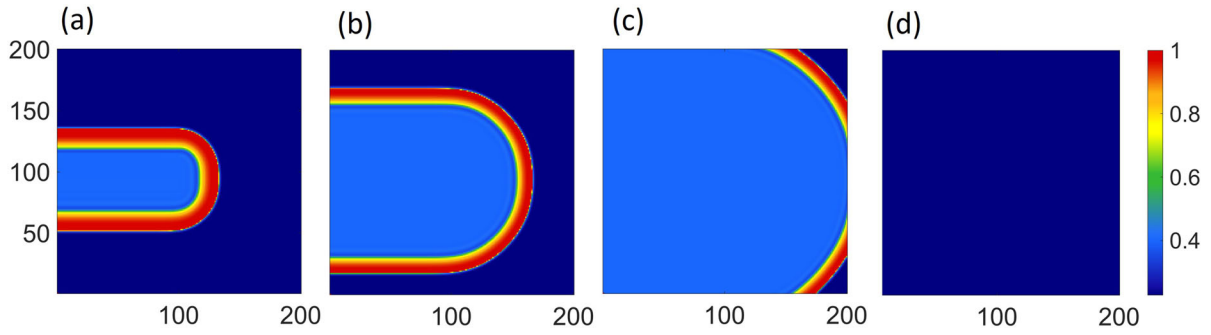

Fig. 4 Low firing threshold of $\theta = 0.1$ fails to generate spiral patterns: The rest of the synaptic parameter setting is as $g_c = 0.02$ and $V_{\text{rev}} = 2.5$. Default values of $k_0 = 0.1$ and $I_{\text{ext}} = 0$ are taken. **a** The slope of the sigmoidal function is adjusted to $\lambda = 40$ to enhance the likelihood of planar oscillators generating propagating waves. Over time, the plane silences at a state of equilibrium. (Color figure online)

reaching higher voltage peaks, as evident from the red coloring indicative of high voltage.

The findings in Figs. 1, 2, and 3 indicate a correlation between the chosen spike threshold θ and the critical value of the sigmoidal slope λ. For the birth of spiral rotors, synapses with thresholds of $\theta = 0.4, 0.25$, and 0.15 require λ to reach the minimum values of 9, 11, and 17, correspondingly. It can be inferred that as the firing threshold decreases, there is a greater need for the sigmoid function to mimic the abrupt transition of a step function through higher λ values.

In general, spiral rotors do not appear when λ falls below the required minimum value. Below the critical λ, several distinct scenarios are likely to take place. When the firing threshold is set as high as $\theta = 0.4$, the localized initial condition effectively stimulates the neighboring silent nodes, resulting in the curvature of the traveling wave's tip. However, this bent tip fails to evolve into a spiral locus and eventually departs from the plane as it propagates outward. By lowering the firing threshold to $\theta = 0.25$, the tip of the traveling wave initially experiences curvature for a limited number of iterations before it brakes and leaves the plane as a simple traveling pulse. In scenarios involving even a lower threshold of $\theta = 0.15$, not only does the wave's tip remain uncurved, but it also remains at its initial site. As a result, the entire lattice is silenced after a few iterations. Conversely, above the critical λ, spiral rotors consistently emerge. These rotors are characterized by a stable reentrant wave tip, gradually establishing dominance over the entire plane as a spiral wave pattern unfolds. Notably, increasing λ corresponds to elevated voltage levels within the wavefronts.

The last and lowest threshold voltage considered in this work is $\theta = 0.1$. As perceived before, a lower threshold demands a higher λ. Thus, in Fig. 4, we set λ to a high value of $\lambda = 40$. Figure 4a–d represents the snapshots taken as t = 40, 80, 140, and 200. As depicted, reducing θ to $\theta = 0.1$ eliminates the capability of localized excited initial conditions to generate spiral patterns.

Note that an increase in the present value of coupling strength, $g_c = 0.02$, may alter the previous results. Our findings in Figs. 1, 2, and 3 demonstrate that a higher reversal potential leads to a smoother sigmoidal function, supporting reentrant tip formation. As the coupling intensity grows, even milder sigmoid slopes effectively promote spiral wave formation. It is important to note that this increase in coupling strength is not universal. For instance, in the case of $\theta = 0.4$, reentrant tips are unattainable for $g_c = 0.05$, even at a high slope of $\lambda = 40$. For $\theta = 0.25$ and 0.15, the limit for spiral formation is even lower. However, the results in Fig. 4, where $\theta = 0.1$, remain unaffected by the increase of coupling strength, and no spiral pattern emerges.

3.2 Birth of spiral waves: the effect of the reversal potential V_{rev}

The reversal potential of a synapse is a voltage level where the inward and outward currents balance each other out, resulting in no net flow of ions across the membrane. The ions' intracellular and extra-

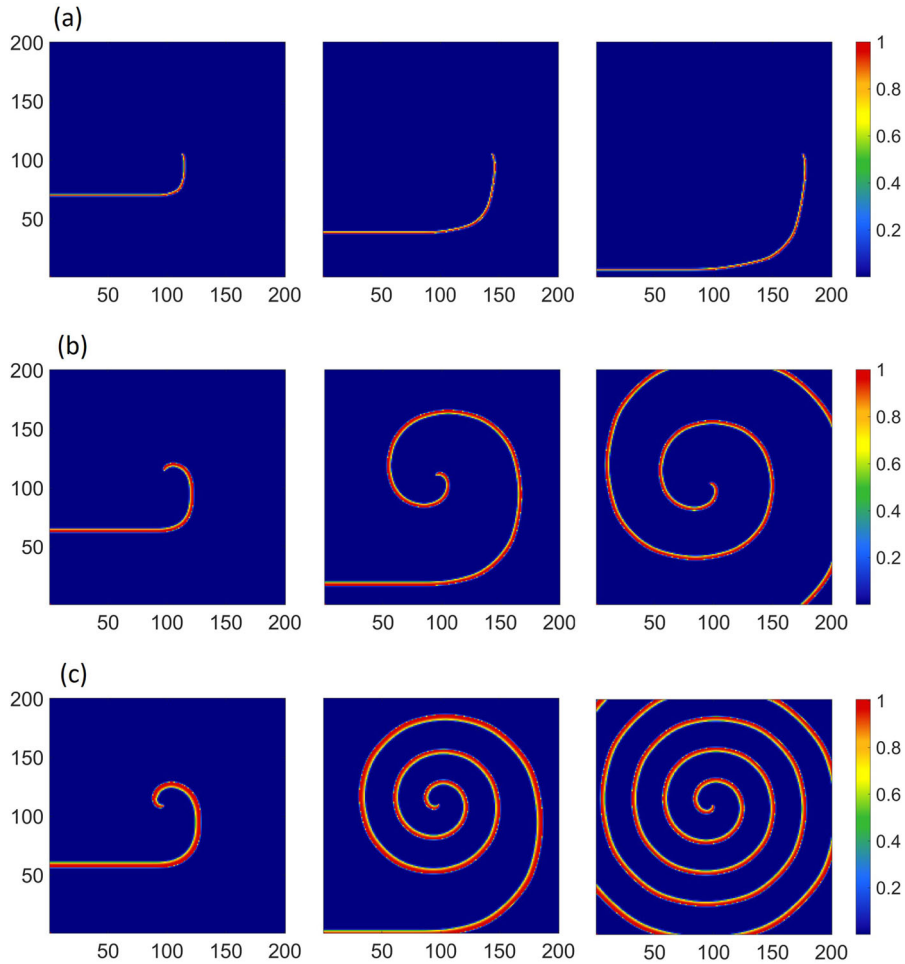

Fig. 5 Effect of reversal potential on the birth of spiral waves: the rest of chemical synapse parameters are $g_c = 0.02$, $\theta = 0.25$, and $\lambda = 35$. Default values of $k_0 = 0.1$ and $I_{\text{ext}} = 0$ are taken. **a** $V_{\text{rev}} = 1.6$ fails to generate a stable reentrant core, **b** $V_{\text{rev}} = 1.9$ a stable core appears and succeeds in generating sustained traveling spiral waves, **c** $V_{\text{rev}} = 2.2$ circular wavefronts of the spiral pattern are spatially closer and are higher in voltage

cellular concentrations are fundamental factors that adjust the reversal potential. The literature suggests that the reversal potential of synaptic currents through neurotransmitter-gated channels tends to shift when exposed to different ionic compositions [45].

In the subsequent section, we focus on evaluating the influence of the reversal potential for excitatory synapses as the condition $V_{\text{rev}} > u_{ij}(t)$ is satisfied. Note that as we have $u_{ij}(t) \leq 1$, any V_{rev} exceeding $V_{\text{rev}} = 1$ establishes an excitatory synapse. The rest of the coupling setting is as $g_c = 0.02, \theta = 0.25$ and $\lambda = 35$. The patterns generated by setting $V_{\text{rev}} = 1.6,\ 1.9$, and 2.2 are presented in Fig. 5a–c, respectively. Different snapshots of traveling waves are provided at t = 100, 200, and 500. In Fig. 5a where $V_{\text{rev}} = 1.6$, the curved wave tip cannot achieve spatial stability and self-reentrance. However, as we increase the reversal potential of excitatory synapse to $V_{\text{rev}} = 1.9$, spiral rotors are shaped as exhibited in Fig. 5b. Figure 5c suggests that the formation of spiral patterns is enhanced as we take $V_{\text{rev}} = 2.2$. By referring to Eq. 3, one might assume that as well as g_c, the magnitude of the term $\left(u_{ij} - V_{\text{rev}}\right)$ may contribute to the strength of coupling. By raising g_c to $g_c = 0.03$ while maintaining $V_{\text{rev}} = 1.6$, stable reentrant waves emerge. Consequently, as long as $V_{\text{rev}} > u_{ij}(t)$, elevating value of V_{rev} acts as if we have increased the strength of synaptic connections.

3.3 Death of spiral waves: the effect of additive external forcing I_{ext}

In general, spiral waves experience instability when subjected to a specific threshold of external forcing current [29]. Inspired by these discoveries, we initially

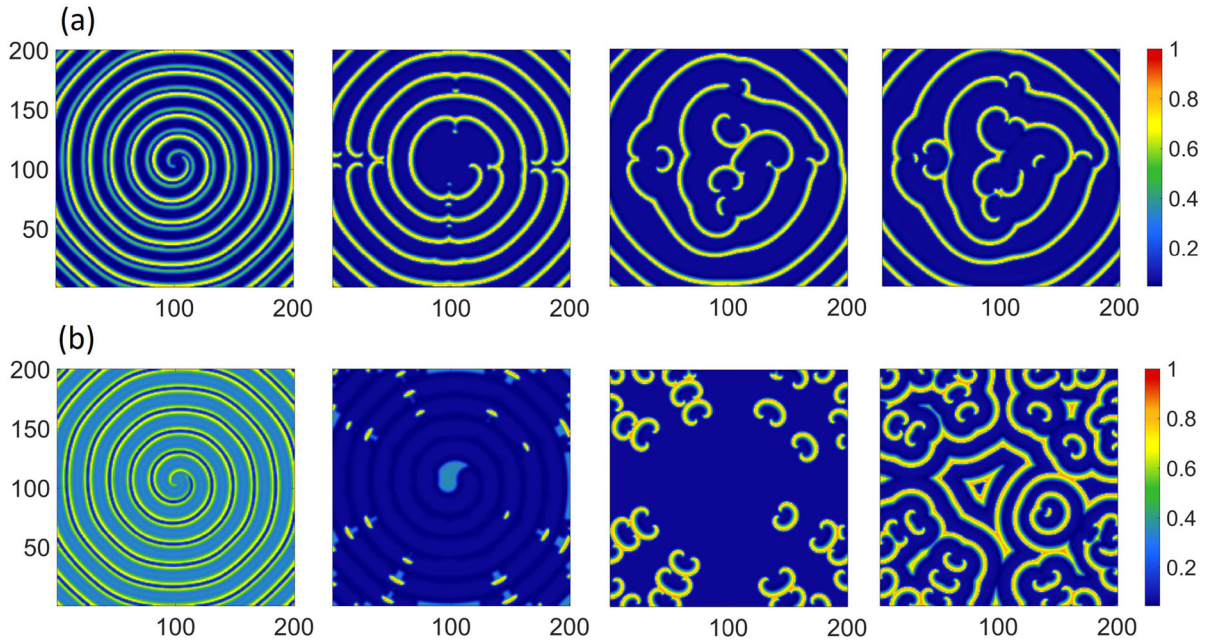

Fig. 6 Destabilization of the single-core spiral wave by applying external current I_{ext}. The birth of turbulent patterns terminates spiral waves. The coupling setting is as $g_c = 0.03$, $\theta = 0.25$, and $\lambda = 35$. The entire lattice is exposed to $I_{\text{ext}} = 0.08$. Default value of $k_0 = 0.1$ is taken. The initial single-core spiral pattern is suppressed. **a** By $V_{\text{rev}} = 2.5$, few scattered spiral seeds appear, and collision of wavefronts end up in turbulences. **b** By $V_{\text{rev}} = 2.7$, spiral seeds are arranged in counter-rotating pairs. The final pattern is turbulent

created a stable spiral pattern by fine-tuning synapse parameters to $g_c = 0.03$, $\theta = 0.25$, and $\lambda = 35$. Here, the reversal potential is treated as a control parameter; however $V_{\text{rev}} \geq 2.5$ is certified. Upon injecting external direct current up to $I_{\text{ext}} = 0.075$, the spiral pattern remains intact. Nevertheless, the circular traveling wavefronts lose their proximity and propagate over longer distances concerning each other. As the external current is set to $I_{\text{ext}} = 0.08$, the traveling spiral wave is accompanied by the emergence of local reentrant seeds. Eventually, these seeds collide with the original rotor, leading to its termination. Hereafter, by taking $I_{\text{ext}} = 0.08$, the death of the initial single-core spiral wave and the emergence of subsequent spatiotemporal patterns are analyzed. We examine four scenarios involving V_{rev} values of 2.5, 2.7, 2.834 and 2.85. By the last value, planar arrays undergo synchronous suppression.

In Fig. 6a, where $V_{\text{rev}} = 2.5$, injection of current $I_{\text{ext}} = 0.08$ destabilizes the original reentrant tip, and a few scattered spiral seeds appear in the plane. The snapshots of membrane potential u are taken at $t = 25$, $t = 60$, $t = 75$, and $t = 105$. Over time, waves emerging from stable seeds collide, giving rise to a turbulent pattern. By elevating reversal potential to $V_{\text{rev}} = 2.7$, the initial spiral pattern is entirely suppressed in early iterations, as depicted in Fig. 6b. However, several pairs of spiral seeds with opposed handedness or rotational direction appear over time. These could be termed mini-spiral rotors, given that the wave tips are more concave than their counterparts discussed earlier in this paper. The exact mechanism through which a single-core spiral with a particular chirality leads to the emergence of counter-rotating seeds remains unidentified. Continuing with temporal simulations of the lattice, we identify turbulent waves originating from the collision of propagating waves generated by mini-spiral rotors. In Fig. 6b, the snapshots of membrane potential u are taken at $t = 25$, $t = 35$, $t = 50$, and $t = 75$.

Figure 7a illustrates the outcomes corresponding to $V_{\text{rev}} = 2.834$. The snapshots of membrane potential u are taken at $t = 25$, $t = 60$, $t = 75$, and $t = 200$. This particular value was selected because it offers insights into generating another spatiotemporal pattern,

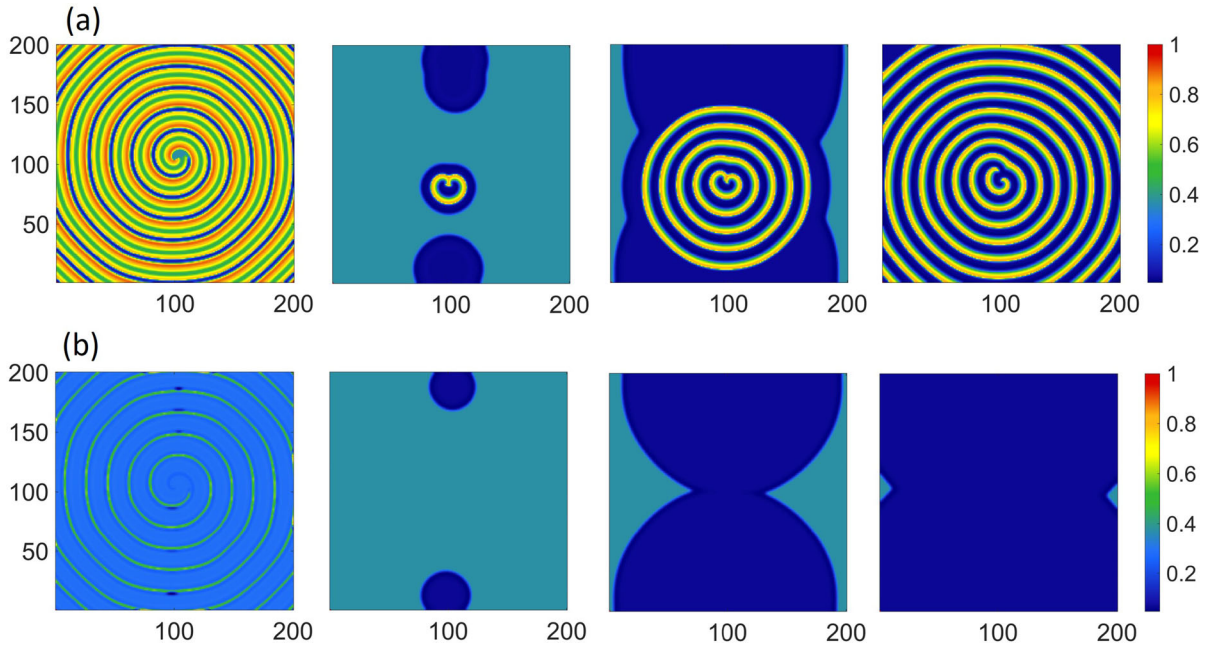

Fig. 7 Destabilization and termination of the single-core spiral wave by applying an external current I_{ext}. Reduction in the number of counter-rotating seeds and the onset of synchronous silence. The coupling setting is as $g_c = 0.03$, $\theta = 0.25$, and $\lambda = 35$. The entire lattice is exposed to $I_{\text{ext}} = 0.08$. Default values of $k_0 = 0.1$ is taken. The initial single-core spiral pattern is terminated. **a** By $V_{\text{rev}} = 2.834$, a centered target wave is born from two spiral rotors with opposed chirality. **b** By $V_{\text{rev}} = 2.85$, the entire lattice falls into a state of synchronized rest

target waves. These patterns are characterized by waves originating from a central point continuously radiating outward. As shown in Fig. 7a, the spiral pattern diminishes first, and then two counter-rotating seeds appear. A resultant target wave is generated upon colliding these two approximate counter-rotating fronts. Note that the counter-rotating seeds are also presented in Fig. 6b, where $V_{\text{rev}} = 2.7$. However, by increasing the reversal potential to $V_{\text{rev}} = 2.834$, the coupling intensity is amplified, and the rotor count is decreased to two. Such observations are also mentioned in the literature. A single-core spiral wave is deemed to take over the network as coupling intensity exceeds a certain threshold; otherwise, a cluster of spiral seeds arises within the network [46]. This statement is supported by the comparisons of outcomes in Figs. 6b and 7a. Note that we have assumed that as long as $V_{\text{rev}} > u_{ij}(t)$ is certified, both V_{rev} and g_c tune coupling strength. Lastly, in Fig. 7b, by making a slight increase up to $V_{\text{rev}} = 2.85$, the previous stable rotors vanish, and the entire lattice synchronizes in equilibrium. In this case, the snapshots of membrane potential u are taken at $t = 25$, $t = 60$, $t = 75$, and $t = 105$.

3.4 Death of spiral waves: the effect of Faradic current induced by memristor

The temporal evolution of the transmembrane potential is determined by a collective of currents introduced through diverse mechanisms. Within the memristive FitzHugh–Nagumo (FHN) model, the magnetic flux emerging from ion exchange across the membrane is represented as the third variable φ. The term $k_0\rho(\varphi)u$ causes variation in the magnetic flux and denotes the induced Faradic current by Faraday's law of electromagnetic induction [47]. As indicated by Eq. 1, the gain of the Faradic current can be managed by adjusting the $k0$ parameter. Previously, the potential of magnetic flux manipulation to destabilize and transform cardiac spiral waves into safer target waves have been highlighted [24,48]. Thus, in the subsequent section, we seek to analyze the effect of the modulating membrane poten-

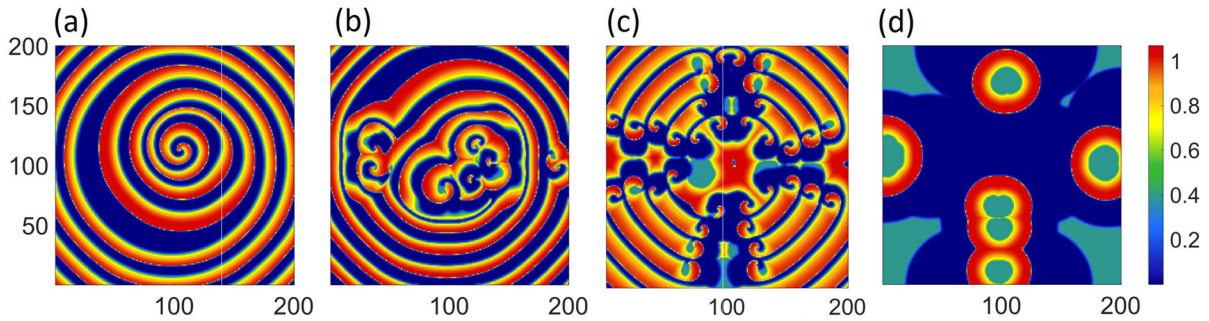

Fig. 8 Destabilization and death of spiral waves altering the gain of memristor-induced Faradic current through parameter k_0. The coupling setting is as $g_c = 0.025$, $\theta = 0.25$, $V_{\text{rev}} = 2.5$, and $\lambda = 35$. External direct current is set back to $I_{\text{ext}} = 0$. **a** $k_0 = 1$, **b** $k_0 = 3$, **c** $k_0 = 3.4$, **d** $k_0 = 3.8$. Through amplifying the Faradic current by memristor weight k_0, the spiral core disappears, giving rise to turbulent traveling waves and eventually silence as $k_0 = 3.8$

tial through intracellular magnetic radiation on the stability of a single-core reentrant wave. We assess our objective by changing the gain of current induced by the flux-controlled memristor through the parameter k_0.

Initially, we generate a centered single-core spiral wave by setting chemical synapse parameters to $g_c = 0.025$, $\theta = 0.25$, $V_{\text{rev}} = 2.5$, and $\lambda = 35$. The external direct current is set back to zero. In the formation of spiral wave, $k_0 = 0.1$ was set. Elevating the value of k_0 enhances the destabilization of reentrant waves by amplifying the effect of electromagnetic induction on the membrane's potential. Figure 8 illustrates the resulting changes in the centered single-core spiral by turning k_0 into 1, 3, 3.4, and 3.8. The snapshots were taken at $t = 100$.

In Fig. 8a, the Faradic gain is raised to $k_0 = 1$. While the spatiotemporal arrangement remains consistent, the pattern's geometry becomes asymmetrical concerning the central rotor. Supposedly, the given k_0 is not strong enough to make the initial spiral wave unstable, as its seed survives. For the spiral rotor to experience instability, the Faradic current is amplified by $k_0 = 3$. Under such conditions, the emergent scattered turbulent seeds overtake the main central rotor, as depicted in Fig. 8b. Some mini-spiral seeds manifest in pairs with opposing handedness, although most exist as solitary entities. As Fig. 8c suggests, when we set $k_0 = 3.4$, the former scattered rotors undergo a significant transformation, replaced by a greater quantity of symmetrical, counter-rotating spiral rotors. Counter-rotating pairs were also observed during the destabilization induced by external current, suggesting a potential emerging pattern in the route of spiral waves' death. Complete elimination of the spiral pattern happens when $k_0 = 3.8$. The snapshot in Fig. 8d exhibits the temporary patterns emerging after the dissolution and before the entire lattice enters a state of silence. Note that the wavefronts are magnified in voltage in the abovementioned scenarios, as the red coloring suggests.

4 Discussion and conclusion

The current study focused on the emergence and suppression of spiral wave patterns within a 200×200 lattice of chemically coupled memristive FitzHugh–Nagumo (FHN) neurons. This work builds upon previous research, which predominantly explored diffusive coupling mechanisms. We restricted the radius of interaction to the eight nearest neighbors within the lattice. Initially, we examined the conditions under which spiral waves could form by manipulating the critical parameters of a chemical synapse: firing threshold, sigmoidal slope, and reversal potential. The sigmoidal function describes the neurotransmitter release mechanism, which exhibits threshold-like behavior. In the context of physiological conditions, we explored scenarios where the firing threshold of synaptic elements tends to be hyperpolarized. Within the voltage range of a FitzHugh–Nagumo (FHN) neuron, we employed various threshold values. In each case, we experimentally manipulated the slope of the sigmoidal function to identify the critical value that gives rise to the formation of spiral rotors. Finally, we evaluated the impact of the third key component of chemical coupling, namely the reversal potential. Upon identifying the optimal cou-

pling configuration that led to a stable, single-core spiral pattern, we evaluated the impact of two destabilizing variables: external direct current and Faradaic current induced by memristive effects. We sought to determine whether currents could destabilize reentrant waves and entirely suppress them, particularly when interactions occurred through chemical synapses.

The results identified that all chemical coupling compartments potentially affect spiral wave birth. By the numerical assessment of sigmoidal slope, which modulates the speed of synaptic response and saturation, we found that a critical value of slope corresponds to each threshold. Stable spiral rotors consistently emerged above the critical value, characterized by reentrant wave tips that gradually dominated the entire lattice. The findings suggested that as the excitability of media is enhanced by reducing the response threshold, a more steep sigmoid function is required. Conversely, below this critical value, the lattice remained silent or incapable of forming stable spirals, depending on the initial firing threshold. The reversal potential also influenced wave tips' spatial stability and self-reentrance. Specifically, the wave tips failed to achieve spatial stability at lower values. However, increasing the reversal potential led to the formation of stable spiral rotors. Based on the chemical synapse description, we deemed that the reversal potential modulates synaptic strength as the coupling intensity coefficient does.

We also examined the destabilizing effects of external direct and memristive Faradic currents. Both factors elevated the excitation level of media as wavefronts were amplified in the traveling voltage value. A specific value of external current was determined to destabilize the original reentrant tip. Intensifying the synaptic connection through the help of reversal potential contributed to suppressing the initial single-core wave. Then, the possibility of the birth of a few scattered spiral seeds appeared. The results confirmed that the emergent rotating cores tended to be less in number as the coupling intensity was raised. Interestingly, the emergent seeds were mostly counter-rotating pairs. The opposite chiralities of seeds in a proper approximation gave rise to symmetrical spatiotemporal patterns known as target waves. All the rotors vanished by a final increase in reversal potential, and the entire lattice synchronized in equilibrium. The Faradaic current caused similar destabilizing effects. First, the pattern's geometry became asymmetrical by amplifying the Faradic gain. The initial single-core spiral was terminated by further amplification, and counter-rotating seeds were born. At the final value of Faradic gain, all spiral rotors were suppressed.

Analogies exist between the birth of spiral waves in networks of chemically coupled neurons and those in electrically coupled neurons. In electric synapses, the intensity of coupling must be finely tuned for traveling waves to form a spiral pattern [49]. When the internodal coupling intensity increases, spiral rotors become unstable [46]. Thus, there is a critical range of coupling intensity necessary for the formation of spiral waves in networks of electrically coupled neurons. In our current study, we shifted our focus to chemical synapses, which possess inherently more complex dynamics. The parameters defining internodal communication in these synapses are more varied, be it the slope of the sigmoid activation function or the firing threshold. Similar to electrical synapses, for the birth of spiral waves, each parameter requires a specific numerical setting. However, tuning these settings is more complicated, as one setting correlates with another. Setting the firing threshold too low disrupts the formation of stable rotors, much like excessively increasing the electrical coupling strength does. Throughout our paper, we specifically investigated two coupling intensities that didn't result in destabilization. Nonetheless, our experiments suggest that similar outcomes can be achieved by increasing the chemical coupling intensity.

Regarding the death of spiral waves, the phenomenon of spirals breaking up into multiple counter-rotating cores can also be observed in electrically coupled networks. In one study, external current stimulation was provided with both a DC component and an added AC term [50]. In another study, colored Gaussian noise served as the source of stimulation [51]. Electromagnetic radiation also serves as a relevant external stimulus. In studies focusing on electrical synapses as the primary coupling mechanism, the stability of spirals has been investigated. One study indicates that adjusting the intensity of electrical coupling changes the necessary external stimuli level to keep spirals stable [52]. A similar conclusion is drawn from another study that assesses the impact of magnetic induction gain, presented as additive memristive feedback [53]. Thus, the spiral waves in neuronal structures, regardless of the type of synaptic connection, may undergo destabilization when an external source of perturbation is exerted.

Funding This work was partially funded by Centre for Nonlinear Systems, Chennai Institute of Technology, India, vide funding number CIT/CNS/2023/RP/012. M.P. was supported by the Slovenian Research and Innovation Agency (Javna agencija za znanstvenoraziskovalno in inovacijsko dejavnost Republike Slovenije) (Grant Nos. P1-0403 and N1-0232).

Data availability This manuscript has no associated data.

Declarations

Conflict of interest The authors declare that they have no conflict of interest.

References

1. Calim, A., Palabas, T., Uzuntarla, M.: Stochastic and vibrational resonance in complex networks of neurons. Philos. Trans. R. Soc. A **379**(2198), 20200236 (2021)
2. Agaoglu, S., Calim, A., Hövel, P., Ozer, M., Uzuntarla, M.: Vibrational resonance in a scale-free network with different coupling schemes. Neurocomputing **325**, 59–66 (2019)
3. Uzuntarla, M.: Firing dynamics in hybrid coupled populations of bistable neurons. Neurocomputing **367**, 328–336 (2019)
4. Atasoy, S., Deco, G., Kringelbach, M., Pearson, J.: Harmonic brain modes: a unifying framework for linking space and time in brain dynamics. Neuroscientist **24**(3), 277–293 (2018)
5. Rakshit, S., Majhi, S., Kurths, J., Ghosh, D.: Neuronal synchronization in long-range time-varying networks. Chaos **31**(7), 073129 (2021)
6. Fries, P.: Rhythms for cognition: communication through coherence. Neuron **88**(1), 220–235 (2015)
7. Sato, T., Nauhaus, I., Carandini, M.: Traveling waves in visual cortex. Neuron **75**(2), 218–229 (2012)
8. Chae, Y., Park, H.-J., Hahm, D.-H., Lee, B.-H., Park, H.-K., Lee, H.: Spatiotemporal patterns of neural activity in response to electroacupuncture stimulation in the rodent primary somatosensory cortex. Neurol. Res. **32**(1), 64–68 (2010)
9. Alamia, A., VanRullen, R.: Alpha oscillations and traveling waves: signatures of predictive coding? PLoS Biol. **17**, 1–26 (2019)
10. Destexhe, A.: Oscillations, complex spatiotemporal behavior, and information transport in networks of excitatory and inhibitory neurons. Phys. Rev. E **50**(2), 1594 (1994)
11. Boucher-Routhier, M., Thivierge, J.-P.: A deep generative adversarial network capturing complex spiral waves in disinhibited circuits of the cerebral cortex. BMC Neurosci. **24**(1), 22 (2023)
12. Troy, W., Shusterman, V.: Patterns and features of families of traveling waves in large-scale neuronal networks. SIAM J. Appl. Dyn. Syst. **6**(1), 263–292 (2007)
13. Liou, J.-Y., Smith, E., Bateman, L., Bruce, S., McKhann, G., Goodman, R., Emerson, R., Schevon, C., Abbott, L.: A model for focal seizure onset, propagation, evolution, and progression. Elife **9**, e50927 (2020)
14. Ten Tusscher, K., Panfilov, A.: Cell model for efficient simulation of wave propagation in human ventricular tissue under normal and pathological conditions. Phys. Med. Biol. **51**(23), 6141 (2006)
15. Witkowski, F., Leon, L., Penkoske, P., Giles, W., Spano, M., Ditto, W., et al.: Spatiotemporal evolution of ventricular fibrillation. Nature **392**(6671), 78–82 (1998)
16. Franović, I., Perc, M., Todorović, K., Kostić, S., Burić, N.: Activation process in excitable systems with multiple noise sources: large number of units. Phys. Rev. E **92**(6), 062912 (2015)
17. Bačić, I., Yanchuk, S., Wolfrum, M., Franović, I.: Noise-induced switching in two adaptively coupled excitable systems. Eur. Phys. J. Spec. Top. **227**, 1077–1090 (2018)
18. Feng, Y., Khalaf, A., Alsaadi, F., Hayat, T., Pham, V.-T.: Spiral wave in a two-layer neuronal network. Eur. Phys. J. Spec. Top. **228**, 2371–2379 (2019)
19. Bukh, A., Strelkova, G., Anishchenko, V.: Spiral wave patterns in a two-dimensional lattice of nonlocally coupled maps modeling neural activity. Chaos Solitons Fractals **120**, 75–82 (2019)
20. Parastesh, F., Rajagopal, K., Alsaadi, F., Hayat, T., Pham, V.-T., Hussain, I.: Birth and death of spiral waves in a network of Hindmarsh–Rose neurons with exponential magnetic flux and excitable media. Appl. Math. Comput. **354**, 377–384 (2019)
21. Huang, L., Ma, J., Tang, J., Li, F.: Transition of ordered waves in neuronal network induced by diffusive poisoning of ion channels. J. Biol. Syst. **21**(1), 1350002 (2013)
22. Hu, B., Ma, J., Tang, J.: Selection of multiarmed spiral waves in a regular network of neurons. PLoS ONE (2013). https://doi.org/10.1371/journal.pone.0069251
23. Ma, J., Liu, Q., Ying, H., Wu, Y.: Emergence of spiral wave induced by defects block. Commun. Nonlinear Sci. Numer. Simul. **18**(7), 1665–1675 (2013)
24. Tabi, C., Etémé, A., Kofané, T.: Unstable cardiac multi-spiral waves in a FitzHugh–Nagumo soliton model under magnetic flow effect. Nonlinear Dyn. **100**, 3799–3814 (2020)
25. Xu, Y., Jia, Y., Ge, M., Lu, L., Yang, L., Zhan, X.: Effects of ion channel blocks on electrical activity of stochastic Hodgkin–Huxley neural network under electromagnetic induction. Neurocomputing **283**, 196–204 (2018)
26. Zhou, X., Xu, Y., Wang, G., Jia, Y.: Ionic channel blockage in stochastic Hodgkin–Huxley neuronal model driven by multiple oscillatory signals. Cognit. Neurodyn. **14**, 569–578 (2020)
27. Rajagopal, K., Jafari, S., Moroz, I., Karthikeyan, A., Srinivasan, A.: Noise induced suppression of spiral waves in a hybrid FitzHugh–Nagumo neuron with discontinuous resetting. Chaos **31**(7), 073117 (2021)
28. Wang, Q., Perc, M., Duan, Z., Chen, G.: Delay-enhanced coherence of spiral waves in noisy Hodgkin–Huxley neuronal networks. Phys. Lett. A **372**(35), 5681–5687 (2008)
29. Jun, M., He-Ping, Y., Yong, L., Shi-Rong, L.: Development and transition of spiral wave in the coupled Hindmarsh–Rose neurons in two-dimensional space. Chin. Phys. B **18**(1), 98 (2009)
30. Kang, Y., Chen, Y., Fu, Y., Wang, Z., Chen, G.: Formation of spiral wave in Hodgkin–Huxley neuron networks with

gamma-distributed synaptic input. Commun. Nonlinear Sci. Numer. Simul. **83**, 105112 (2020)
31. Rajagopal, K., Karthikeyan, A., Jafari, S., Parastesh, F., Volos, C., Hussain, I.: Wave propagation and spiral wave formation in a Hindmarsh–Rose neuron model with fractional-order threshold memristor synaps. Int. J. Mod. Phys. B **34**(17), 2050157 (2020)
32. Majhi, S., Bera, B., Bhowmick, S., Ghosh, D.: Restoration of oscillation in network of oscillators in presence of direct and indirect interactions. Phys. Lett. A **380**(43), 3617–3624 (2016)
33. Rossoni, E., Chen, Y., Ding, M., Feng, J.: Stability of synchronous oscillations in a system of Hodgkin–Huxley neurons with delayed diffusive and pulsed coupling. Phys. Rev. E **71**(6), 061904 (2005)
34. Rouach, N., Avignone, E., Meme, W., Koulakoff, A., Venance, L., Blomstrand, F., Giaume, C.: Gap junctions and connexin expression in the normal and pathological central nervous system. Biol. Cell **94**(7–8), 457–475 (2002)
35. Majhi, S., Perc, M., Ghosh, D.: Chimera states in uncoupled neurons induced by a multilayer structure. Sci. Rep. **6**(1), 39033 (2016)
36. Viana, R., Borges, F., Iarosz, K., Batista, A., Lopes, S., Caldas, I.: Dynamic range in a neuron network with electrical and chemical synapses. Commun. Nonlinear Sci. Numer. Simul. **19**(1), 164–172 (2014)
37. Wang, R., Li, J., Du, M., Lei, J., Wu, Y.: Transition of spatiotemporal patterns in neuronal networks with chemical synapses. Commun. Nonlinear Sci. Numer. Simul. **40**, 80–88 (2016)
38. Feng, P., Wang, R., Wu, Y.: Critical Behaviors of Regular Pattern Selection in Neuronal Networks with Chemical Synapses, pp. 163–171. Springer, Berlin (2020)
39. Ma, J., Wang, Y., Wang, C., Xu, Y., Ren, G.: Mode selection in electrical activities of myocardial cell exposed to electromagnetic radiation. Chaos Solitons Fractals **99**, 219–225 (2017)
40. Foster, K., Kreitzer, A., Regehr, W.: Interaction of postsynaptic receptor saturation with presynaptic mechanisms produces a reliable synapse. Neuron **36**(6), 1115–1126 (2002)
41. Acuna, C., Guo, Q., Burré, J., Sharma, M., Sun, J., Südhof, T.: Microsecond dissection of neurotransmitter release: SNARE-complex assembly dictates speed and Ca^{2+} sensitivity. Neuron **82**(5), 1088–1100 (2014)
42. Tang, A., Hong, I., Boddington, L., Garrett, A., Etherington, S., Reynolds, J., Rodger, J.: Low-intensity repetitive magnetic stimulation lowers action potential threshold and increases spike firing in layer 5 pyramidal neurons in vitro. J. Neurosci. **335**, 64–71 (2016)
43. Bera, B., Ghosh, D., Banerjee, T.: Imperfect traveling chimera states induced by local synaptic gradient coupling. Phys. Rev. E **94**(1), 012215 (2016)
44. Yu, D., Lu, L., Wang, G., Yang, L., Jia, Y.: Synchronization mode transition induced by bounded noise in multiple time-delays coupled FitzHugh–Nagumo model. Chaos Solitons Fractals **147**, 111000 (2021)
45. Otis, T., Raman, I., Trussell, L.: AMPA receptors with high Ca^{2+} permeability mediate synaptic transmission in the avian auditory pathway. J. Physiol. **482**(2), 309–315 (1995)
46. Ma, J., Hu, B., Wang, C., Jin, W.: Simulating the formation of spiral wave in the neuronal system. Nonlinear Dyn. **73**, 73–83 (2013)
47. Wu, F., Wang, C., Xu, Y., Ma, J.: Model of electrical activity in cardiac tissue under electromagnetic induction. Sci. Rep. **6**(1), 28 (2016)
48. Rostami, Z., Jafari, S., Perc, M., Slavinec, M.: Elimination of spiral waves in excitable media by magnetic induction. Nonlinear Dyn. **94**, 679–692 (2018)
49. Wu, X., Ma, J., Li, F., Jia, Y.: Development of spiral wave in a regular network of excitatory neurons due to stochastic poisoning of ion channels. Commun. Nonlinear Sci. Numer. Simul. **18**(12), 3350–3364 (2013)
50. Ma, J., Wang, C.-N., Jin, W.-Y., Wu, Y.: Transition from spiral wave to target wave and other coherent structures in the networks of Hodgkin–Huxley neurons. Appl. Math. Comput. **217**(8), 3844–3852 (2010)
51. Ma, J., Jia, Y., Tang, J., Yang, L.: Breakup of spiral waves in coupled Hindmarsh–Rose neurons. Chin. Phys. Lett. **25**(12), 4325 (2008)
52. Tabi, C., Etémé, A., Kofané, T.: Unstable cardiac multi-spiral waves in a FitzHugh–Nagumo soliton model under magnetic flow effect. Nonlinear Dyn. **100**, 3799–3814 (2020)
53. Yang, Z., Zhang, Y., Wu, F.: Memristive magnetic coupling feedback induces wave-pattern transition. Nonlinear Dyn. **100**, 647–658 (2020)